Combustion Theory and Modelling
Vol. 11, No. 4, August 2007, 639–652

Taylor & Francis
Taylor & Francis Group

Numerical and experimental observations of spherical diffusion flames

K. J. SANTA†, Z. SUN‡, B. H. CHAO*†, P. B. SUNDERLAND§,
R. L. AXELBAUM‡, D. L. URBAN¶ and D. P. STOCKER¶

†Department of Mechanical Engineering, University of Hawaii at Manoa, Honolulu, HI 96822, USA
‡Department of Mechanical and Aerospace Engineering, Washington University,
St. Louis, MO 63130, USA
§Department of Fire Protection Engineering, University of Maryland, College Park, MD 20742, USA
¶NASA Glenn Research Center, Cleveland OH 44135, USA

(Received 27 June 2006; in final form 4 November 2006)

Spherical diffusion flames supported on a porous sphere were studied numerically and experimentally. Experiments were performed in 2.2 s and 5.2 s microgravity facilities. Numerical results were obtained from a Chemkin-based programme. The programme simulates flow from a porous sphere into a quiescent environment, yields both steady state and transient results and accounts for optically thick gas-phase radiation. The low flow velocities and long residence times in these diffusion flames lead to enhanced radiative and diffusive effects. Despite similar adiabatic flame temperatures, the measured and predicted temperatures varied by as much as 700 K. The temperature reduction correlates with flame size but characteristic flow times and Lewis number also influence temperature. The numerical results show that the ambient gas Lewis number would have a strong effect on flame temperature if the flames were steady and nonradiating. For example, a 10% decrease in Lewis number would increase the steady state flame temperature by 200 K. However, for these transient, radiating flames the effect of Lewis number is small. It was also observed that when hydrocarbon fuel is supplied from the ambient the large diffusion distances associated with these flames can lead to unusual steady state compositions near the outer boundary because decomposition products can diffuse to the outer boundary. This results in a loss of chemical enthalpy from the system but the effect on flame temperature is small. Transient predictions of flame sizes are larger than those observed in microgravity experiments. Close agreement could not be obtained without either increasing the model's thermal and mass diffusion properties by 30% or reducing mass flowrate by 25%.

Keywords: Laminar spherical diffusion flames; Lewis number; Microgravity; Numerical combustion; Thin-filament pyrometry

1. Introduction

Spherical diffusion flames are valuable tools for understanding nonpremixed combustion [1–5]. These flames are one-dimensional and are straightforward to model. The flames can be generated in microgravity using droplets or by issuing a gaseous or liquid reactant from a porous sphere. Unique features of the flame supported on a porous sphere include the ability to select the direction of convection from fuel to oxidizer (normal flame) or from oxidizer to

*Corresponding author. E-mail: bchao@eng.hawaii.edu

Combustion Theory and Modelling
ISSN: 1364-7830 (print), 1741-3559 (online)
http://www.tandf.co.uk/journals
DOI: 10.1080/13647830601161567

fuel (inverse flame) for given fuel and oxidizer concentrations (i.e. for a given stoichiometric mixture fraction, Z_{st}). The flames can have extremely low scalar dissipation rates, approaching those of purely diffusion (zero convection) flames.

Spherical diffusion flames have been employed to study the effects of Z_{st} on soot production [4] and sooting limits [5]. These results have shown, as have earlier works [2], that the flames may not reach steady state during 2.2 s or even 5.2 s of microgravity. These flames generally have small scalar dissipation rates, which result in long times to reach steady state. Furthermore, small scalar dissipation rates result in large radiative losses from the gaseous products, which can significantly reduce flame temperatures compared to normal-gravity flames. To obtain a better understanding of the factors influencing transient spherical flames, and thus allow a clearer interpretation of past and future data, a systematic numerical study was undertaken to consider the influence of flow direction, stoichiometric mixture fraction, radiative heat loss and Lewis number (Le) on flame temperatures and sizes of spherical diffusion flames. Also considered is reactant loss by diffusion of intermediates away from the flame when the flame burns in a fuel environment. In addition, measurements of the flame temperature and location were made in NASA's 2.2 s and 5.2 s drop facilities to assess the accuracy of the numerical results.

Flame structure can be influenced by the direction of convection across the flame (convection direction) and stoichiometric mixture fraction. The convection direction (either into the oxidizer or the fuel) is controlled by the selection of burner and ambient gases, while the stoichiometric mixture fraction is controlled by varying the amount of inert (e.g. nitrogen) in the fuel and/or oxidizer. Four ethylene flames have been studied, namely those considered in our earlier work [4], and they are described in table 1. The four flames have the same adiabatic flame temperature, 2370 K, which is that of neat ethylene burning in air when the reactants are supplied at 300 K. They also have the same ethylene consumption rate, 1.51 mg/s. A schematic diagram and sample images of these flames are shown in reference [4]. Table 1 includes characteristic residence times, t_{res}, defined as the estimated mass of gas between the flame and the burner divided by the burner mass flowrate [5].

In a spherical diffusion flame, only the Lewis number of the ambient gas (not that of the burner gas) has a significant effect on the flame [6–8]. For spherical flames burning in air this Le is near unity, but for inverse flames it depends on fuel properties and can deviate from unity. Since in this study the ambient gas composition is varied, we are able to study the influence of Le on these flames. The effect of Le could be significant in low-strained flames because diffusion distances will be greater and thus effects of unequal diffusion rates will be more pronounced. Law and Chung found that for a one-dimensional chamber flame and a stagnation-point flame, blowing reduces the effects of Le when it follows the direction of diffusion and increases the effects when it opposes diffusion [6]. The analytical theory showed that for a non-radiating one-dimensional chamber flame, a 10% reduction or increase in the Le from unity of the reactant supplied against the flow results in a 9% increase or 5% decrease in flame temperature. This is a much more significant effect than that observed in strained systems so one of the goals of the current study is to determine if this effect can be realized in microgravity spherical flames.

2. Numerical

In the model a gaseous reactant is injected from the porous spherical burner at temperature T_b into an infinite quiescent environment of the other reactant at temperature T_∞. The burner is assumed to be perfectly symmetric so that the flow field and flame are spherically symmetric in microgravity. The numerical code is a modification of the PREMIX [9] code, adapted to a diffusion flame in a spherical geometry and allowing for optically thick radiative heat losses.

For this problem, the equations describing the conservation of mass, energy and gas species are

$$\frac{\partial \rho}{\partial t} + \frac{1}{r^2}\frac{\partial (r^2 \rho u)}{\partial r} = 0 \tag{1}$$

$$\rho c_p \frac{\partial T}{\partial t} = \frac{1}{r^2}\frac{\partial}{\partial r}\left(r^2 \lambda \frac{\partial T}{\partial r}\right) - \rho u c_p \frac{\partial T}{\partial r} - \sum_{k=1}^{K}\left(\rho c_{p,k} Y_k V_k \frac{\partial T}{\partial r} + h_k \omega_k Y_k\right) - Ra \tag{2}$$

$$\rho \frac{\partial Y_k}{\partial t} = -\frac{1}{r^2}\frac{\partial}{\partial r}\left(r^2 \rho Y_k V_k\right) - \rho u \frac{\partial Y_k}{\partial r} + W_k \omega_k Y_k, \quad k = 1, 2, \ldots, K \tag{3}$$

where T is the temperature, Y_k is the mass fraction of species k, W_k is the molecular weight of species k, t is time, r is the radial spatial coordinate, u is the radial flow velocity, ρ is the gas density, c_p is the averaged specific heat at constant pressure, λ is the heat conductivity, h_k is the specific enthalpy of species k, $c_{p,k}$ is the specific heat of species k, V_k is the diffusion velocity of species k, ω_k is the production rate of species k, K is the number of species and Ra is the rate of radiative heat loss. The equations were solved subject to the following boundary conditions

$$r = r_b : T = T_b; \quad Y_k(u + V_k) = u Y_{k,0}, \quad k = 1, 2, \ldots, K \tag{4}$$

$$r \to \infty : T \to T_\infty; \quad Y_k \to Y_{k,\infty}, \quad k = 1, 2, \ldots, K \tag{5}$$

where the subscripts 0, b and ∞ refer to conditions at the centre of the burner, the burner surface and the ambient, respectively. Because thermocouple measurements in the 5.2 s drop facility showed no significant increase in burner surface temperature during the drop, T_b was taken to be constant. In addition, the results indicate that after 5 s the thermal field had only reached a radius of 9 cm from the centre of the burner and the computations predicted no significant change in reactant compositions at a radius of 100 cm. Thus, while the computations assumed a finite domain ($r_{wall} = 100$ cm), it was effectively infinite and the results were not affected by this assumption. Both T_b and T_∞ were taken to be 300 K in this study.

Radiation was considered to be optically thick and caused only by the participation of CO_2, H_2O and CO. The radiative properties of these gases were formulated by a statistical narrow-band model with a spectral bandwidth of 25 cm^{-1}. The emissivities were extracted from the line-by-line values given by the HITRAN database [10]. To account for the angular variation of the radiation intensity, the discrete ordinates method was employed, with a discrete representation that included 20 different directions. The rate of radiative heat transfer was then evaluated by integrating over all directions using Gaussian quadrature. A more detailed description of the radiation model can be found in [11].

Conventional finite difference techniques with non-uniform mesh spacing were adopted for the discretization of the differential equations. The transient terms were expressed by a forward difference formula, the diffusive terms by a central difference formula, and, for better convergence, the convective terms by an upwind difference formula. The discretized equations were solved by Sandia's Twopnt package [12], which uses Newton's method to solve transient and steady state boundary value problems. The chemical reaction rates, the thermodynamic properties, and the transport properties were evaluated by Chemkin and Transport software [13, 14]. The kinetics data were provided by GRI-Mech 3.0, which contains 53 species and 325 reactions [15]. The number of grids was varied until the solution did not change with further addition of grids. The time step was adjusted until the solution converged.

Following the approach adopted in [2], the initial (ignition) conditions for the transient cases were prescribed as the steady state solutions of flames without radiation and with the

same outer boundary values, but with the outer boundary brought to 1.2 cm from the burner exit. The temperature boundary condition at the burner exit was adiabatic. These conditions lead to a thin high-temperature ignition source near the burner surface, which is consistent with the conditions that would exist when a diffusion flame is first established after ignition (i.e. the gradients are steep and radiative losses are negligible).

3. Experimental

The experiments were conducted in microgravity in the NASA Glenn Research Center 2.2 s and 5.2 s drop facilities. The experimental apparatus is described in detail in Sunderland *et al.* [4, 5]. The burner was a 6.4 mm diameter porous stainless-steel sphere. All tests were conducted in a pressure vessel of 26 l initially at 0.98 bar (with an estimated uncertainty of $\pm$ 0.005 bar) and room temperature.

Each test involved three gases: a hydrocarbon fuel (typically ethylene), nitrogen, and oxygen. Purity of the fuels was 99.9% while that of nitrogen and oxygen was 99.999%. The test conditions are summarized in tables 1 and 2. For each test either fuel or oxygen was diluted with nitrogen. The various gas mixtures were prepared either gravimetrically or by partial-pressure mixing and had an estimated composition uncertainty of $\pm$ 0.001 mole fraction. Both normal and inverse flames were considered, where the pressure vessel was initially filled with, respectively, oxidizer and fuel.

Burner gas flowrates were measured under steady state, cold flow conditions in normal gravity about 30 min (for 2.2 s tests) or 90 min (for 5.2 s tests) before drop initiation. These flowrates were measured with a calibrated mass flowmeter and were adjusted with a needle valve. Uncertainties in the burner flowrates are estimated at $\pm$ 10%. At 2 s before drop initiation the two solenoid valves were opened to commence flow to the burner. The ignitor was energized in microgravity immediately after drop initiation and ignited the flames within 30 ms.

The flames were imaged using two cameras. For tests that did not involve thin-filament pyrometry (TFP) a colour charge-coupled device (CCD) video camera was used. This camera had 640 $\times$ 480 pixels, 8 bits per colour plane, a framing rate of 30 Hz, and a 16 mm manual-iris lens at f/1.4. Spatial resolution was 150 μm. The camera yielded flame appearance and average radius from ignition until drop termination. Except for flame (c), flame radii were measured using the contours of peak blue emission in the video records. For flame (c) only yellow (not blue) emissions were visible. Thus the radii for flame (c) were measured using the inside of the contours of brightest yellow emissions. Flame diameters were determined by averaging the longest chord through each flame and its perpendicular chord; radii were then obtained by dividing the results by two.

For tests involving thin-filament pyrometry (in the 2.2 s drop tower) the video camera was replaced with a Nikon D100 consumer-grade colour digital still camera. This camera has a CCD with 3008 $\times$ 2000 pixels (6 megapixels) and 12 bits per colour plane. The lens that was used has a focal length of 60 mm and was set at f/8. Exposure time was 33 ms, ISO was 200, white balance was direct sunlight, and all automatic gain and focusing were disabled. Spatial resolution was 27 μm. Images from this camera were used to determine approximate peak temperatures and flame radii.

The TFP method used here was based on past work [16–18]. Three silicon carbide fibers, with diameters of 13.9 μm, were strung across the flames in the camera focal plane. Before each test they were heated to glowing in lean regions of a diffusion flame to remove any deposited soot. A solenoid triggered the shutter release, whereby the camera recorded four images at times of 0.1, 0.7, 1.3 and 1.9 s after drop initiation. The filament images were

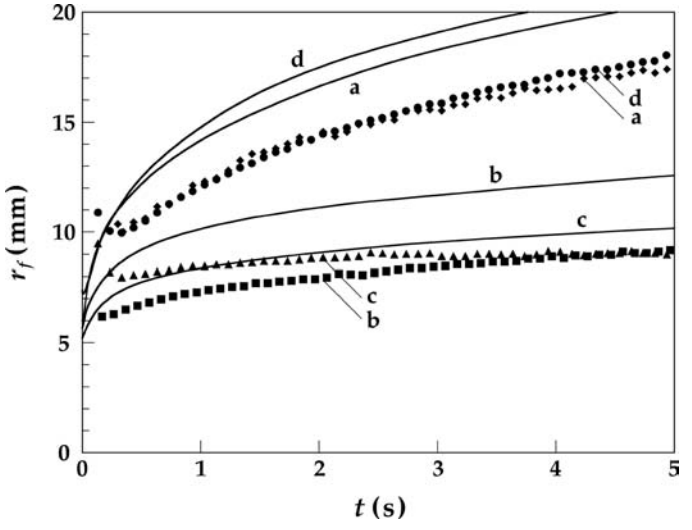

Figure 1. Predicted and measured flame radii for four ethylene flames: (a) C_2H_4 issuing into 21% O_2, (b) 8.14% C_2H_4 issuing into O_2, (c) 21% O_2 issuing into C_2H_4, and (d) O_2 issuing into 8.14% C_2H_4. The curves are numerical results while the symbols represent experiments in the 5.2 s drop facility. The modelled radii correspond to peak temperatures. The measurements were derived from video records.

smoothed using 5 × 5 pixel binning. The brightest pixel greyscale was then recorded along each of the six fibre-flame crossings and these were averaged. These average greyscales were converted to relative fibre temperatures using the previous calibration for a similar TFP system of 0.215 K/greyscale [18]. These fibre temperatures were corrected for radiative loss [18]. An absolute temperature reference was obtained by a thermocouple measurement of the peak temperature for flame (d) at 1.9 s [4]. The TFP temperatures were repeatable but have high estimated uncertainties of ± 150 K owing to calibration uncertainties, slight soot deposition on the fibres, and incipient saturation in the red colour plane for the methane test.

4. Results and discussion

4.1 *Numerical and experimental*

Computations were performed for ethylene flames (a)–(d), defined in table 1. Figure 1 shows measured and predicted flame radii of these flames. The flame radius from the model was assumed to be the radius of the peak temperature. As can be seen from figure 1 all flames initially grew with time, but flames (b) and (c) approached steady state more rapidly than flames (a) and (d) because of their high flow velocities and low residence times (see table 1). The initial growth can be understood from the fact that diffusion flames stabilize where the fluxes of oxidizer and fuel are in stoichiometric proportions. For the present transient flames,

Table 1. Test conditions for ethylene flames (a)–(d).

Flame	Burner gas	Ambient gas	$X_{C_2H_4}$	X_{O_2}	$Y_{C_2H_4}$	Y_{O_2}	Z_{st}	m_b, mg/s	t_{res}, s
(a)	C_2H_4	O_2/N_2	1	0.21	1	0.233	0.064	1.51	2.19
(b)	C_2H_4/N_2	O_2	0.0814	1	0.0815	1	0.78	18.6	0.046
(c)	O_2/N_2	C_2H_4	1	0.21	1	0.233	0.064	22.2	0.091
(d)	O_2	C_2H_4/N_2	0.0814	1	0.0815	1	0.78	5.18	0.893

the consumption of the ambient reactant over time reduces the gradient and thus the flux to the flame. In response, the flames expand to reduce the burner reactant flux at the flame. The rate of variation of flame radii with time predicted by the model matches the experiments for flame (b) after about 0.5 s and for flames (a) and (d) after about 1 s. The initial difference in slopes is likely owing to differences in initial (ignition) conditions between the model and experiments. The measured luminous radii of flame (c) match the predicted flame radii. However the measured radii are only estimates because they were based on yellow emissions.

While the trends for flames (a), (b), and (d) predicted by the model closely resemble those of the experiments, the model predicts larger flames. A similar discrepancy was observed in a previous study [2] and was accounted for by noting that the peak temperature occurs on the oxidizer side of the visible flame. Although this explanation would improve the agreement for flames (a) and (b), it would reduce the agreement for flames (c) and (d). The source of the discrepancy remains unclear, but it could arise from thermal and mass diffusion properties that are too low in the model or from experimental flowrates that are lower than reported, or a combination of both. Transport properties are based on the Lennard–Jones potential model [19], which can underpredict transport properties of light species by up to 25% [20, 21].

To evaluate the effect of assumed transport properties, the thermal and mass diffusion properties in the model were varied. Figure 2 shows the results when transport properties were increased 30% above the values predicted by the Transport code [14] for flames (a), (b), and (d). Flame (c) was not included in figure 2 owing to uncertainties in flame radius resulting from soot obscuration. Because both transport properties were increased, the Lewis number and the adiabatic flame temperature were unchanged. The agreement between model and experiment in figure 2 is improved by this change. A similar improvement is observed following a reduction of 25% in the model's mass flowrate, but this exceeds the 10% estimated uncertainty in the experimental flowrate. Because the source of discrepancy between experiment and theory is unknown, the unmodified transport properties are used in the remainder of this work.

Predictions of transient peak flame temperatures for the four ethylene-fuelled flames are shown in figure 3. Owing to gaseous radiative heat loss the peak temperatures are predicted to decrease with time except near ignition. Although these four flames have the same adiabatic flame temperature (2370 K), the temperatures of flames (a) and (d) are predicted to be markedly

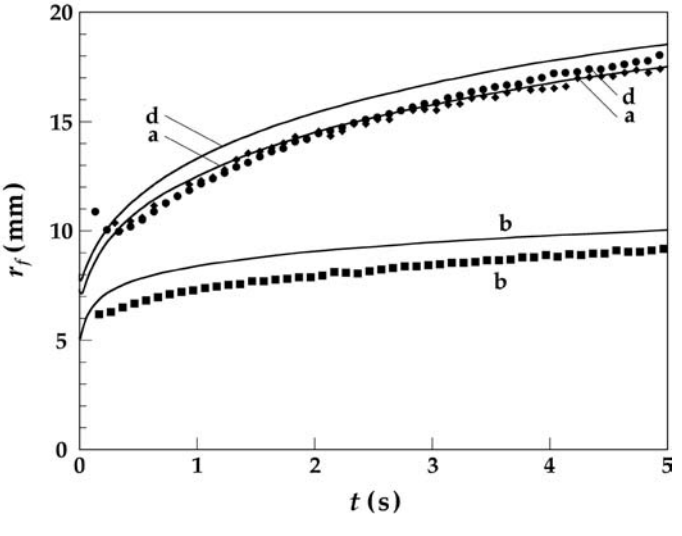

Figure 2. A comparison similar to figure 1, where the transport properties have been increased by 30% in the model and flame (c) has been omitted.

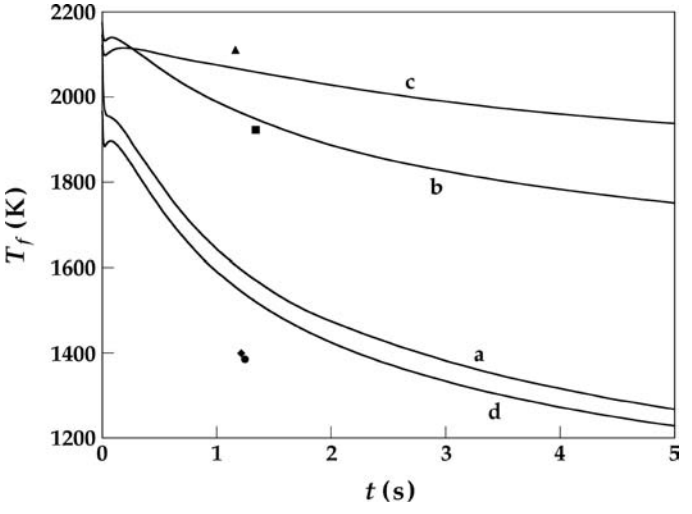

Figure 3. Evolution of peak flame temperature with time for ethylene flames (a)–(d). The curves represent transient numerical results while the symbols represent thermocouple measurements in the 2.2 s drop tower, with legend as given in figure 1.

lower than those of flames (c) and (b). As shown in figure 1, flames (a) and (d) have roughly double the radii of the other flames. The larger flames have greater radiative losses, resulting in peak temperatures up to 700 K cooler than the other flames. In fact, even though these flames are quite different structurally, one being a low Z_{st} normal flame and the other a high Z_{st} inverse flame, they both have similar temperatures, indicating the dominant effect of flame size on radiative heat loss. However, flame size is not the sole factor affecting flame temperature. Comparison of flame temperatures of flames (a) and (b) at a flame radius of 10 mm reveals a 115 K difference in flame temperature for the same flame radius. The higher temperature of flame (b) is likely attributable to its shorter residence time (see table 1) as a result of its higher flowrate.

Also shown in figure 3 are peak temperatures for these four flames as measured with thermocouples in the 2.2 s drop tower. Each symbol indicates an average temperature (previously reported in reference [4]) and an average measurement time (not previously reported) from repeat tests. These temperatures are radiation-corrected with estimated uncertainties of $\pm$ 50 K [4]. The agreement between modelled and measured temperatures is within experimental uncertainties for flames (b) and (c). The numerical predictions in the other two flames significantly over-predict the measured temperatures and this probably arises from different ignition conditions in the model and the experiment. For example, in the experiments there are about 2 s of reactant flow through the porous sphere before ignition. This results in a premixed flame that rapidly transitions to a diffusion flame but leaves products behind that enhance radiation and reduce flame temperature, which is consistent with the lower experimental temperature for flames (a) and (d). Such differences are not evident for flames (b) and (c) because the effects of ignition are convected outward more rapidly in those flames. These flames have a larger mass flowrate and a smaller flame radius, leading to much shorter characteristic residence times (see table 1).

To understand the basic structural differences in the four flames without the complexity of transient effects and radiative heat loss, *steady state* calculations without radiation were performed using the same code, and the results are plotted in figure 4. Because there is no heat loss to the burner in this simulation, and all four flames have the same equilibrium adiabatic

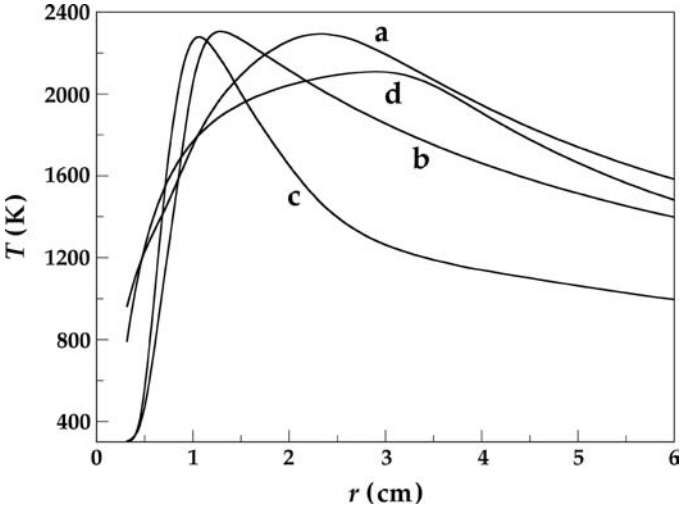

Figure 4. Steady state solutions of the temperature distributions for ethylene flames (a)–(d) without radiative heat loss.

flame temperature (2370 K), these four flames might be expected to have peak temperatures close to 2370 K. This is the case for flames (a)–(c), but flame (d) is about 200 K cooler.

Two factors may cause the reduced peak temperature of flame (d) in this steady simulation. One is that flame (d), unlike flame (b), has fuel in the ambient, which could lead to a loss of intermediate species by diffusion into the ambient. Figures 5 and 6 show, respectively, the distribution of major products and fuel for steady flames (c) and (d). Losses of CO, H_2 and C_2H_2 to the ambient are evident for both flames. Nonetheless, the peak temperature of flame (c) is comparable to that of the normal flames, flames (a) and (b), which do not suffer from loss of intermediates. The flux of intermediates to the ambient is greater in flame (c) than flame (d) so clearly the 200 K reduction in flame temperature for steady flame (d) cannot be a result of the loss of intermediates.

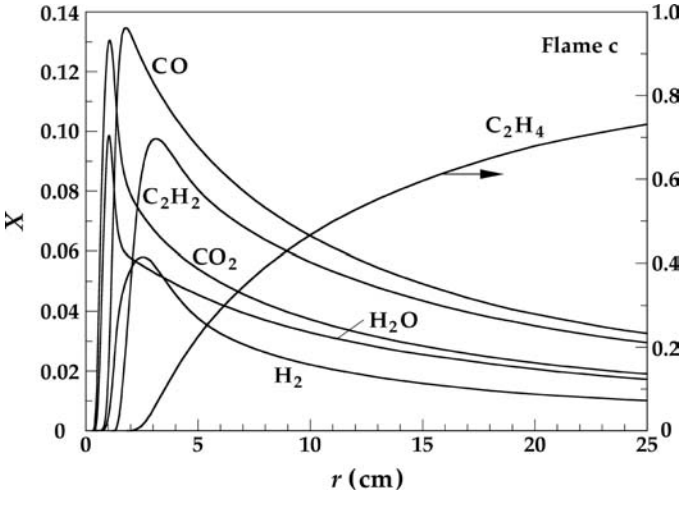

Figure 5. Steady state solutions of major product concentrations without radiative heat loss for ethylene flame (c): 21% O_2 issuing into C_2H_4.

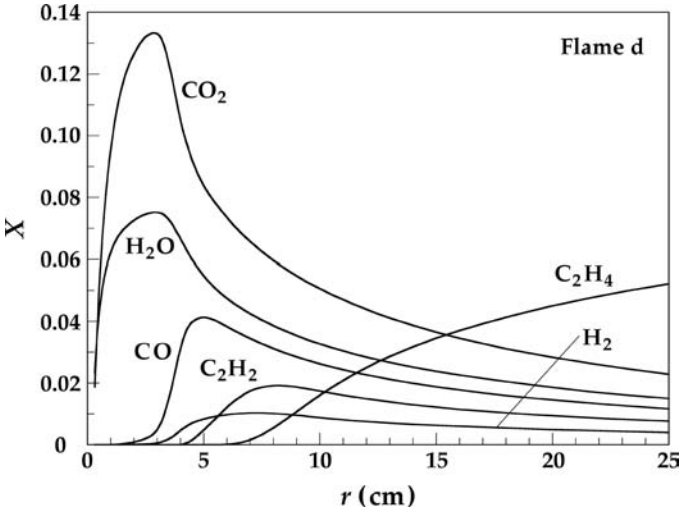

Figure 6. Steady state solutions of major product concentrations without radiative heat loss for ethylene flame (d): O_2 issuing into 8.14% C_2H_4.

A more plausible explanation for the reduced peak temperature of steady flame (d) is that the Lewis number of the ambient reactant for this flame is higher than that of the others. Le is defined here as the mixture thermal diffusivity divided by the mass diffusivity of the reactant in the mixture. It is known that for spherical burner-supported and droplet flames the dominant Le affecting flame temperature is that on the ambient side of the flame [7, 8]. While a reduction in temperature can occur when the ambient Le exceeds unity, a 200 K reduction might be considered large for flame (d).

To observe the effects of non-unity Lewis number of the ambient reactant, computations were performed for flame (d) in steady state using the same code, assuming ambient Le_F equal to, greater than and less than unity, and employing a simplified one-step reaction in the reaction-sheet limit. That is, the reaction rate was set to be sufficiently fast that further increases in reaction rate would not change the solution. The diffusivities for all species were made the same. Computations for Le_F of 0.9, 1.0 and 1.1 were performed and the results are shown in figure 7. With a 10% increase/decrease in Le_F, the flame temperature decreases/increases by about 200 K, in qualitative agreement with Law and Chung [6]. These results suggest that the difference in ambient Le between steady flame (d) and the other flames accounts for the 200 K decrease observed in figure 4. Such Lewis number effect was not observed for the transient flames shown in figures 1 and 3 because of the growth of the flame. The outward expansion of the flame towards the ambient suppresses the significance of inward diffusion (against convection) required for the ambient reactant to reach the flame.

To verify that the Le_F of flame (d) is higher than those of flames (a)–(c), the variation of Le of the ambient reactant for these four flames is shown in figure 8. These results were obtained from the steady state computations using the code described in section 2 but without radiation, as in figures 4 and 5. A distance of 10 cm from the flame sheet was chosen to be the domain of interest because diffusion of the ambient reactant is most important in this preheat region ahead of the flame. In the region of 4–10 cm from the flame there are two groupings: flames (a)–(c) have nearly unity Lewis number and flame (d) has a Lewis number of about 1.2. Closer to the flame, flame (c) shows an increase in Le but because the fuel is in the ambient, the primary fuel already is decomposed here (see figure 5) and thus the relevant Le is no longer that of the fuel, but rather some function of the Le of the intermediates. The intermediates are

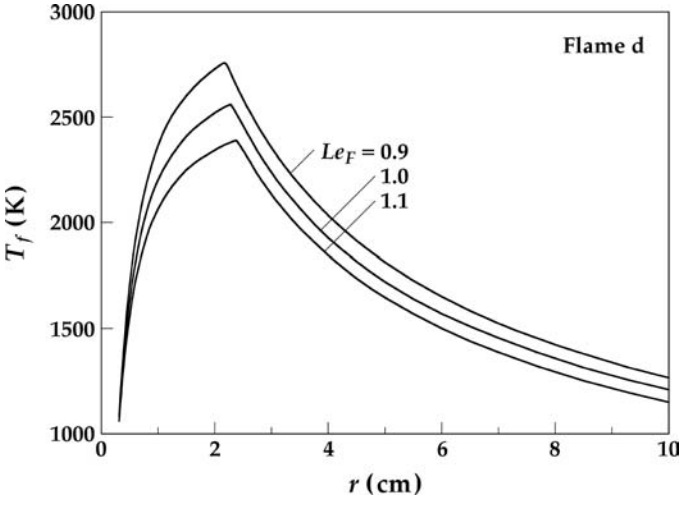

Figure 7. Steady state solution of temperature profiles without radiative heat loss for ethylene flame (d) with Lewis numbers of 0.9, 1.0 and 1.1. A one-step, reaction sheet limit was used in the simulation.

smaller molecules, which have a greater diffusivity and thus a smaller Le. Thus, the primary observation that can be made from figure 8 is that in the diffusion zone approaching the flame, the Le of flame (d) is approximately 20% greater than that of the other flames.

4.2 *Analytical*

An analysis that employs the Burke–Schumann reaction sheet limit was performed for steady inverse flames to better understand the effect of Lewis number. The analysis assumes constant transport properties, but allows different Lewis numbers on the fuel and oxidizer side of the flame. The solution yields the flame temperature, given by

$$T_f = \left(T_0 + \frac{\nu_F W_F}{\nu_O W_O}\frac{q_F}{c_p}Y_{O,0}\right) - \left(T_0 + \frac{\nu_F W_F}{\nu_O W_O}\frac{q_F}{c_p}Y_{O,0} - T_\infty\right)\left(\frac{\nu_F W_F Y_{O,0}}{\nu_F W_F Y_{O,0} + \nu_O W_O Y_{F,\infty}}\right)^{1/Le_F} \tag{6}$$

where ν_k is the stoichiometric coefficient of species k, q_F is the heat of combustion per unit mass of the fuel, T_0 is the supplied gas temperature at the centre of the burner, and the subscripts F and O denote fuel and oxidizer. In equation (6), Le_F is the Lewis number of the fuel/nitrogen mixture, which for flame (d) is the ambient reactant. As expected, the solution of equation (6) indicates that flame temperature depends only on the ambient-side Lewis number. In addition, flame temperature increases/decreases when the ambient Le_F is below/above unity. This analytical finding is consistent with the present numerical results and with earlier studies [6, 7].

The flame temperatures and the relative differences of flame temperature from the unity Lewis number flame for selected hydrocarbon flames, calculated using equation (6) for steady flame (d), are plotted versus Le_F in figure 9. A variation in ambient Le can be affected by changing the ambient diluent (as in figure 7) and/or the fuel. For example, if N_2 were replaced with He here, an increase in Le would result, whereas with CO_2 a decrease would occur. The flame temperatures of the unity Le_F flames are calculated using the Chemical Equilibrium with

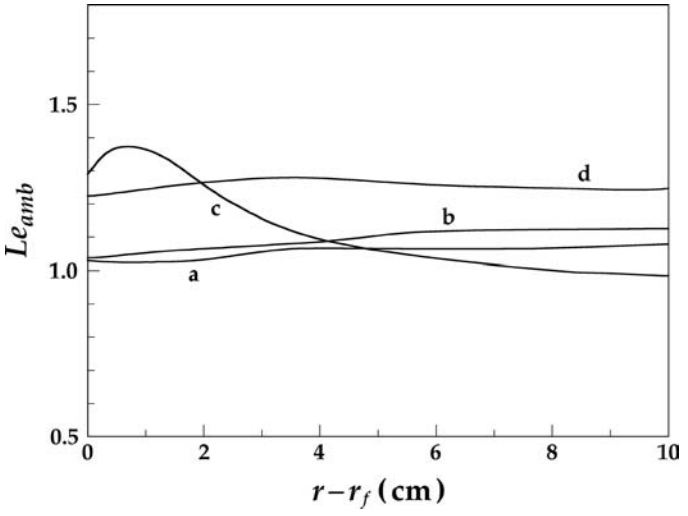

Figure 8. Variation of the Lewis number of the ambient reactant, Le_{amb}, versus the distance from the flame sheet for four ethylene flames. Results shown are for steady state flames without radiative heat loss.

Applications (CEA) code [22]. The value of (q_F/c_p) for each fuel is adjusted such that the flame temperatures obtained from equation (6) agree with those obtained from CEA. Figure 9 shows that all fuels have the same qualitative behavior in that flame temperature decreases with increasing Le. When the flame temperature is normalized relative to the value at unity Le, i.e. $T_f/T_f(\mathrm{Le}_F = 1)$, the data collapse to a single curve, as shown in figure 9, indicating that the relative change of flame temperature is independent of fuel type. Consistent with figure 7, in steady flames when Le_F is near unity a 10% increase in Le_F results in about a 200 K decrease in flame temperature, or about an 8% change. This effect increases with decreasing Lewis number, as previously reported [6].

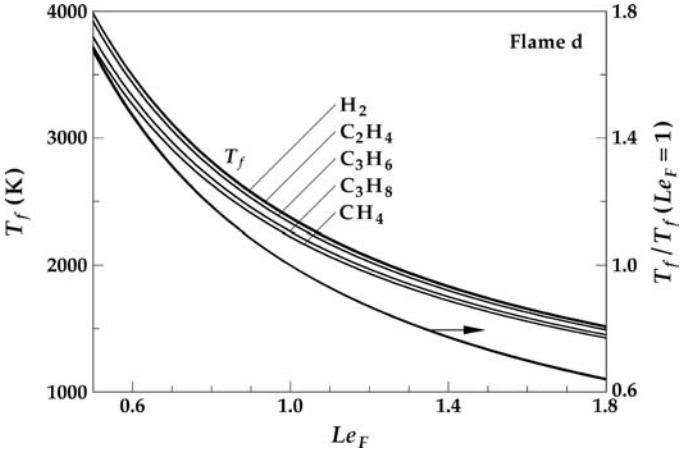

Figure 9. Flame temperature calculated using equation (6) versus Lewis number for flame (d) for selected fuels. The lowest curve represents, for all fuels, the relative change of flame temperature from the unity Lewis number flame.

Table 2. Measured and modelled relative peak temperatures 1.9 s after ignition for inverse flames of three hydrocarbon fuels*.

Burner GAS	Ambient GAS	Le_F† (300 K)	X_F	Y_F	Z_{st}	m_b mg/s	$T_{max} - T_{max,C2H4}$, K Measured	Modelled
O_2	CH_4/N_2	0.92	0.14	0.0853	0.75	5.85	322‡	152
O_2	C_2H_4/N_2	1.37	0.0814	0.0815	0.78	5.18	0	0
O_2	C_3H_8/N_2	1.98	0.058	0.0884	0.76	4.49	− 275	− 117

*Each of these flames has an adiabatic flame temperature of 2370 K. Note that the second flame here is ethylene flame (d).
†The Le_F was estimated from Chemkin [13] where the thermal diffusivity is that of nitrogen and the mass diffusivity is that of the fuel into the fuel mixture.
‡ Lower bound owing to incipient saturation in the thin-film pyrometer.

4.3 *Results for other fuels*

Figure 4, which does not include gaseous radiation, clearly shows the reduction in temperature for flame (d), attributed to Le effects. Nonetheless, this finding is not readily apparent in the experimental and numerical results in figure 3, owing to the different radiative losses in the four flames. Therefore experimental validation of the predicted flame temperature variation with ambient Le was sought. Three flames were studied in the 2.2 s drop tower with the thin-filament pyrometer and were modelled numerically. The flames include ethylene flame (d) and corresponding flames burning methane and propane fuels, as summarized in table 2. Fuel dilution levels were selected such that the adiabatic flame temperatures of the three flames was 2370 K. The ambient Le of the methane flame is less than that of ethylene flame while the ambient Le of the propane flame is higher. Flowrates in table 2 were selected such that the ethylene and propane flame sizes were similar at 1.9 s, but limited access to the drop tower resulted in the methane flame radius being about 10% smaller. Nevertheless, these conditions are expected to yield comparable radiative loss fractions for these flames, and thus the effects of Le can be delineated.

The measured relative temperatures shown in table 2 were determined by TFP. Compared with the ethylene flame, these results reveal that the methane and propane flames have increased and decreased peak temperatures, respectively, as is expected from their ambient Lewis numbers. Transient numerical predictions, also shown in table 2, support these trends. The quantitative agreement between measured and modelled relative temperatures is adequate given uncertainties in the TFP measurements and possible residual ignition effects.

5. Conclusions

Novel aspects of spherical diffusion flames were examined. The work sought theoretical and computational insight into flame size, temperature, gaseous radiation, intermediate species loss, and Lewis number effects for four very different flame types: fuel (ethylene) into air, air into fuel, diluted fuel into oxygen and oxygen into diluted fuel. Where possible, the results were compared with microgravity measurements, emphasizing these four diffusion flames which had different stoichiometric mixture fractions and convection directions.

The transient flame code predicted the temporal development of flame radius in 5 s tests, but accurate prediction of flame sizes were only obtained when transport properties were increased by 30% or when flow rates were decreased by 25%. Spherical flames with various convection directions and stoichiometric mixture fractions (at constant adiabatic flame temperature) reveal that in general there is a decrease in peak temperature with an increase in flame size. This

is attributed to increased gas-phase radiative losses in large flames. Nonetheless, residence time also affects flame temperature. For the inverse spherical diffusion flame, where the fuel is in the ambient, intermediate species can be lost to the ambient, which can result in a small reduction in flame temperature. Finally, ambient Lewis number was found to have a profound effect on flame temperature for flames with long residence times provided that the flames are steady and nonradiating. For example, for Le near unity, a 10% decrease in Le is predicted to increase flame temperature by 200 K in these spherical diffusion flames. Nonetheless, the flame temperature of the unsteady, radiating flames of this study were not strongly affected by Le.

Acknowledgement

This work was supported by NASA Grants NCC3-696 and NCC3-1062 (BHC), NCC3-697 and NCC3-1063 (RLA) and NNC05-AA46A (PBS).

References

[1] Atreya, A. and Agrawal, S., 1998, Effect of radiative heat loss on diffusion flames in quiescent microgravity atmosphere. *Combustion and Flame*, **115**, 372–382.

[2] Tse, S.D., Zhu, D., Sung, C.-J., Ju, Y. and Law, C.K., 2001, Microgravity burner-generated spherical diffusion flames: experiment and computation. *Combustion and Flame*, **125**, 1265–1278.

[3] Christiansen, E.W., Tse, S.D. and Law, C.K., 2003, A computational study of oscillatory extinction of spherical diffusion flames. *Combustion and Flame*, **134**, 327–337.

[4] Sunderland, P.B., Axelbaum, R.L., Urban, D.L., Chao, B.H. and Liu, S., 2003, Effects of structure and hydrodynamics on the sooting behavior of spherical microgravity diffusion flames. *Combustion and Flame*, **132**, 25–33.

[5] Sunderland, P.B., Urban, D.L., Stocker, D.P., Chao, B.-H. and Axelbaum, R.L., 2004, Sooting limits of microgravity spherical diffusion flames in oxygen-enriched air and diluted fuel. *Combustion Science and Technology*, **176**, 2143–2164.

[6] Law, C.K. and Chung, S.H., 1982, Steady state diffusion flame structure with Lewis number variations. *Combustion Science and Technology*, **29**, 129–145.

[7] Chung, S.H. and Law, C.K., 1983, Structure and extinction of convective diffusion flames with general Lewis numbers. *Combustion and Flame*, **52**, 59–79.

[8] Mills, K. and Matalon, M., 1997, Burner-generated spherical diffusion flames. *Combustion Science and Technology*, **129**, 295–319.

[9] Kee, R.J., Grcar, J.F., Smooke, M.D., Miller, J.A. and Meeks, E., 1987, *A Program for Modeling Steady, Laminar, One-Dimensional Premixed Flames*. Report No. SAND85-8240, Sandia National Laboratories.

[10] Rothman, L.S., Rinsland, C.P., Goldman, A., Massie, S.T., Edwards, D.P., Flaud, J.-M., Perrin, A., Camy-Peyret, C., Dana, V., Mandin, J.-Y., Schroeder, J., Mccann, A., Gamache, R.R., Wattson, R.B., Yoshino, K., Chance, K.V., Jucks, K.W., Brown, L.R., Nemtchinov, V. and Varanasi, P., 2003, The HITRAN molecular spectroscopic database: edition of 2000 including updates through 2001. *Journal of Quantitative Spectroscopy and Radiative Transfer*, **82**, 5– 44.

[11] Carlson, B.G. and Lathrop, K.G., 1968, Transport theory - the method of discrete ordinates. In: H. Greenspan, C.N. Kelber and D. Okrent (Eds) *Computing Methods in Reactor Physics* (New York: Gordon and Breach).

[12] Grcar, J.F., 1992, *The Twopnt Program for Boundary Value Problems*. Report No. SAND91-8230, Sandia National Laboratories.

[13] Kee, R.J., Rupley, F.M. and Miller, J.A., 1989, *Chemkin-II: A Fortran Chemical Kinetics Package for the Analysis of Gas Phase Chemical Kinetics*. Report No. SAND89-8009B, Sandia National Laboratories.

[14] Kee, R.J., Dixon-Lewis, G., Warnatz, J., Coltrin, M.E. and Miller, J. A., 1988, *A Fortran Computer Code Package for the Evaluation of Gas Phase Multicomponent Transport Properties*. Report No. SAND86-8246, Sandia National Laboratories.

[15] Smith, G.P., Golden, D.M., Frenklach, M., Moriarty, N.W., Eiteneer, B., Goldenberg, M., Bowman, C.T., Hanson, R.K., Song, S., Gardiner Jr., W.C., Lissianski, V.V. and Qin, Z. Available online at http://www.me.berkeley.edu/gri_mech/.

[16] Vilimpoc, V. and Goss, L.P., 1988, SiC-based thin-filament pyrometry: theory and thermal properties. *Proceedings of the Combustion Institute*, **22**, 1907–1914.

[17] Pitts, W.M., 1996, Thin-filament pyrometry in flickering laminar diffusion flames. *Proceedings of Combustion Institute*, **26**, 1171–1179.

[18] Maun, J.D., Sunderland, P.B. and Urban, D.L., 2007, Thin-filament pyrometry with a digital still camera. *Applied Optics* (in press).
[19] Hirschfelder, J.O., Curtiss, C.F. and Bird, R.B., 1964, *Molecular Theory of Gases and Liquids* (Hoboken: Wiley and Sons).
[20] Paul, P. and Warnatz, J., 1998, A re-evaluation of the means used to calculate transport properties of reacting flows. *Proceedings of the Combustion Institute*, **27**, 495–504.
[21] Middha, P., Yang, B. and Wang, H., 2002, A first-principle calculation of the binary diffusion coefficients pertinent to kinetic modeling of hydrogen/oxygen/helium flames. *Proceedings of the Combustion Institute*, **29**, 1361–1369.
[22] McBride, B.J. and Gordon, S., 1996, *Computer Program for Calculation of Complex Chemical Equilibrium Compositions and Applications*. Report No. RP-1311-P2, NASA Lewis Research Center.